ELSEVIER

Journal of Structural Geology 26 (2004) 847–853

JOURNAL OF STRUCTURAL GEOLOGY

www.elsevier.com/locate/jsg

Numerical simulation of strain within lava domes

Cécile Buisson, Olivier Merle*

Laboratoire Magmas et Volcans, Observatoire de Physique du Globe, 5 rue Kessler, 63038 Clermont-Ferrand, France

Received 8 April 2003; received in revised form 24 October 2003; accepted 11 November 2003

Abstract

A new analytical and numerical method is presented to assess 3D deformation within lava domes. The method allows any simultaneous combination of strain components, even that of a pure shear and six elementary simple shear components. The method's practical use is presented. Model results provide the following information for lava dome strain patterns: in the upper part of a dome stretching is perpendicular to flow direction and in the lower part it is parallel. Flinn parameter values indicate a flattening strain ellipsoid through the dome, except in a small zone in the centre, where it is a constriction ellipsoid.

Keywords: Lava domes; Strain matrix; Numerical simulation; Experiments

1. Introduction

In a recent paper (Buisson and Merle, 2002), analogue experiments have been conducted to assess the displacement and velocity patterns within lava domes. Silicone putty, used to simulate the analogue-magma, was vertically extruded from a reservoir and flowed on a rigid, horizontal base (Fig. 1). The evolving geometry with time has been described in detail and the competing effects of injection and gravity analysed in terms of upward and downward movements within the dome (Buisson and Merle, 2002). Deformation of a square grid has allowed the determination of orientation of the flattening plane in a vertical section.

Following previous studies on strain simulation within geological structures (e.g. Coward, 1976; Brun, 1977; Coward and Kim, 1981; Brun and Burg, 1982; Sanderson, 1982; Sanderson and Marchini, 1984; Merle, 1986; Ellis and Watkinson, 1987; Tikoff and Teyssier, 1994; Jones and Tanner, 1995; Merle and Gapais, 1997), strain pattern can be determined using numerical models involving combinations of simple shear and pure shear components. In this paper, we use strain components and strain gradients inferred from the deformed grid to perform a numerical computation of the 3D strain within natural domes. This 3D approach makes it possible to determine stretching direction versus flow direction and the type of strain ellipsoids in space, which can help in interpreting strain in natural examples.

2. A universal deformation matrix

Strain components as deduced from the deformed grid both in section and at the upper free surface of the 3D experiments are used to propose a general model of the total strain generated in three dimensions of space. Numerical modelling is done with 3D Cartesian co-ordinates having two axes (X and Y) lying along the horizontal basal plane on which spreading occurs. The origin is located above the centre of the feeding conduit (Fig. 1).

In the Buisson and Merle (2002) model, the deformed squares of the grid reveal three main strain components, which vary throughout the model (Fig. 1a). Coaxial shortening or lengthening in the X, Y and Z directions correspond to the first of these major strain components and is referred to as a pure shear component. The three axes (k_X, k_Y, k_Z) of the strain ellipsoid of this pure shear component can be expressed in the following matrix D_{PS} where each point of (x_0, y_0, z_0) co-ordinates before deformation are transformed into points of (x', y', z') co-ordinates after deformation:

$$\begin{pmatrix} x' \\ y' \\ z' \end{pmatrix} = D_{PS} \begin{pmatrix} x_0 \\ y_0 \\ z_0 \end{pmatrix} \quad (1)$$

* Corresponding author. Tel.: +33-4-7334-6732; fax: +33-4-7334-6744.
E-mail addresses: merle@opgc.univ-bpclermont.fr (O. Merle), Elizabethbuisson@aol.com (C. Buisson).

0191-8141/$ - see front matter © 2004 Published by Elsevier Ltd.
doi:10.1016/j.jsg.2003.11.017

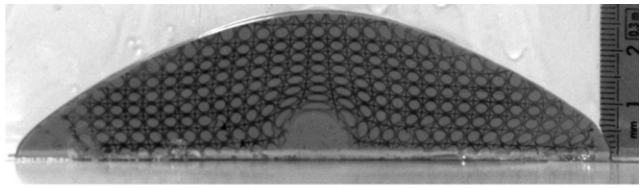

a

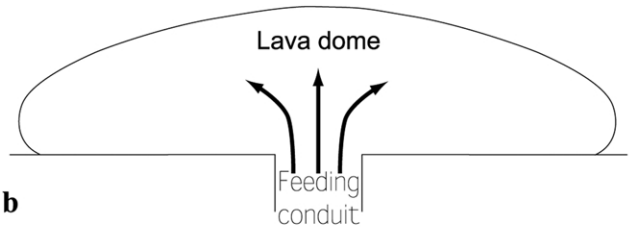

b

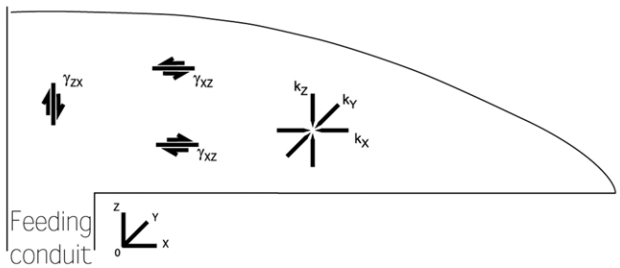

c

Fig. 1. (a) Photograph of a 2D experiment (Buisson and Merle, 2002). (b) Sketch of a lava dome: the magma is injected vertically through a feeding conduit and flows radially on a rigid planar base. (c) Sense of shear of the two simple shear components (γ_{ZX} and γ_{XZ}) and orientations of the pure shear components (k_X, k_Y, k_Z) for the numerical simulation.

with

$$D_{\mathrm{PS}} = \begin{bmatrix} k_X & 0 & 0 \\ 0 & k_Y & 0 \\ 0 & 0 & k_Z \end{bmatrix}$$

Lengthening occurs in the Y direction irrespective of location within the dome as a result of radial displacement (Buisson and Merle, 2002). Everywhere k_Z is a shortening axis. Shortening or lengthening may occur in the X direction depending on the location within the dome.

Vertical and horizontal simple shear components are clear from the deformation of the square grid as described in detail in the experimental paper (Buisson and Merle, 2002). They can be expressed as two simple shear components (γ_{XZ} and γ_{ZX}) acting in the X and Z directions, which can be defined by the following deformation matrices:

$$D_{XZ} = \begin{bmatrix} 1 & 0 & \gamma_{XZ} \\ 0 & 1 & 0 \\ 0 & 0 & 1 \end{bmatrix}$$

and

$$D_{ZX} = \begin{bmatrix} 1 & 0 & 0 \\ 0 & 1 & 0 \\ \gamma_{ZX} & 0 & 1 \end{bmatrix} \quad (2)$$

Strain gradients associated with these three strain components are selected when the model reaches a steady state flow, depending on the strain variations observed from the experimental grid. An important result of the experimental approach is that the sense of shearing of the γ_{XZ} component is reversed in the upper part of the dome (Fig. 1c) (Buisson and Merle, 2002).

The simultaneous combination of the three components can be expressed by the following general deformation matrix:

$$D = \begin{bmatrix} k_X & 0 & \Gamma_{XZ} \\ 0 & k_Y & 0 \\ \Gamma_{ZX} & 0 & k_Z \end{bmatrix} \quad (3)$$

in which the two off-diagonal elements Γ can be called the effective shear deformation in the XZ plane (Tikoff and Fossen, 1993). From previous studies (e.g. Coward and Kim, 1981; Merle, 1986, 1998; Tikoff and Fossen, 1993; Soto, 1997), it is clear that these off-diagonal terms are a function of a combination of the pure and simple shear components:

$$\Gamma = f(\gamma, k) \quad (4)$$

Matrix multiplication in general is non-commutative. This means that the general deformation matrix of Eq. (3) is not the product of the deformation matrices D_{PS}, D_{XZ} and D_{ZX}. Any strain result using the product of these elementary matrices would be demonstrably different from the simultaneous combination of individual strain components.

In 1993, Tikoff and Fossen proposed a general deformation matrix for simultaneous finite pure shear and finite simple shear. This matrix allows the simultaneous combination of some specific thrusting and wrenching components leading to a 3×3 upper triangular matrix. That approach has been successfully used in numerical modelling of strain in lava tubes (Merle, 2000). In our simulation here, vertical shearing in the Z direction makes the matrix different from an upper triangular one so that the deformation matrix proposed by Tikoff and Fossen (1993) could not be used. A general deformation matrix for three dimensions has also been proposed by Soto (1997), but equations are complicated and too long to be managed easily.

In a recent paper, a new numerical method that can be used for any combination of simple shear and pure shear components has been proposed (Provost et al., 2004). We follow herein this numerical method according to the specific case in our experiments, but it is suitable for any simultaneous combination of simple shear and pure shear components. It is outside the scope of this paper to present

the theory explaining this new numerical method, of which full details can be found in Provost et al. (2004). Here we simply show the application of the approach for any simple shear and pure shear combination.

According to Ramberg (1975), the instantaneous strain rate (or incremental) matrix (A) can be calculated taking the logarithm of each finite strain matrix (D) as follows:

$$A_{PS} = \ln(D_{PS}) \tag{5}$$

$$A_{XZ} = \ln(D_{XZ}) \tag{6}$$

$$A_{ZX} = \ln(D_{ZX}) \tag{7}$$

The incremental matrix (A_{SC}) for the simultaneous combination of the three strain components is the sum of each individual incremental matrix:

$$A_{SC} = A_{PS} + A_{XZ} + A_{ZX} \tag{8}$$

Then, the finite deformation matrix for the simultaneous combination under consideration is given by taking the exponential of the incremental matrix A_{SC}:

$$D = e^{A_{SC}} \tag{9}$$

This numerical method may be used with the help of any mathematical software, such as Matlab, which calculates the logarithm and the exponential of a 3×3 matrix. The general solution of the problem is given by the following universal deformation matrix D:

$$D = \exp(\ln D_1 + \ln D_2 + \ldots + \ln D_n) \tag{10}$$

Then, strain can be solved from the symmetrical Finger tensor ($F = D \times D^{t}$; Malvern, 1969, p. 174), which has eigenvalues E_i equal to the principal quadratic elongations and eigenvectors parallel to the principal strain axes. The three principal axes (λ_1, λ_2 and λ_3) of the strain ellipsoid are defined as the square root of the eigenvalues such as $\lambda_i = \sqrt{E_i}$, with $\lambda_1 > \lambda_2 > \lambda_3$. The shape of the strain ellipsoid is given by the Flinn parameter K ($K = [(\lambda_1/\lambda_2) - 1)/(\lambda_2/\lambda_3) - 1]$), for which $K < 1$ and $K > 1$ indicates flattening ($\lambda_1 > \lambda_2 > 1 > \lambda_3$) and constriction ($\lambda_1 > 1 > \lambda_2 > \lambda_3$) type ellipsoids, respectively. Plane strain means no change in the intermediate axis ($\lambda_2 = 1$) and yields $K = 1$.

3. Results

The input parameters in our simulation (k_x, k_y, k_z, γ_{XZ}, γ_{ZX}) are determined from the comparison through time of the deformed grids emplaced both on cross-sections for 2D experiments and on the upper free surface for 3D experiments. This makes it possible to show that k_y and k_z within

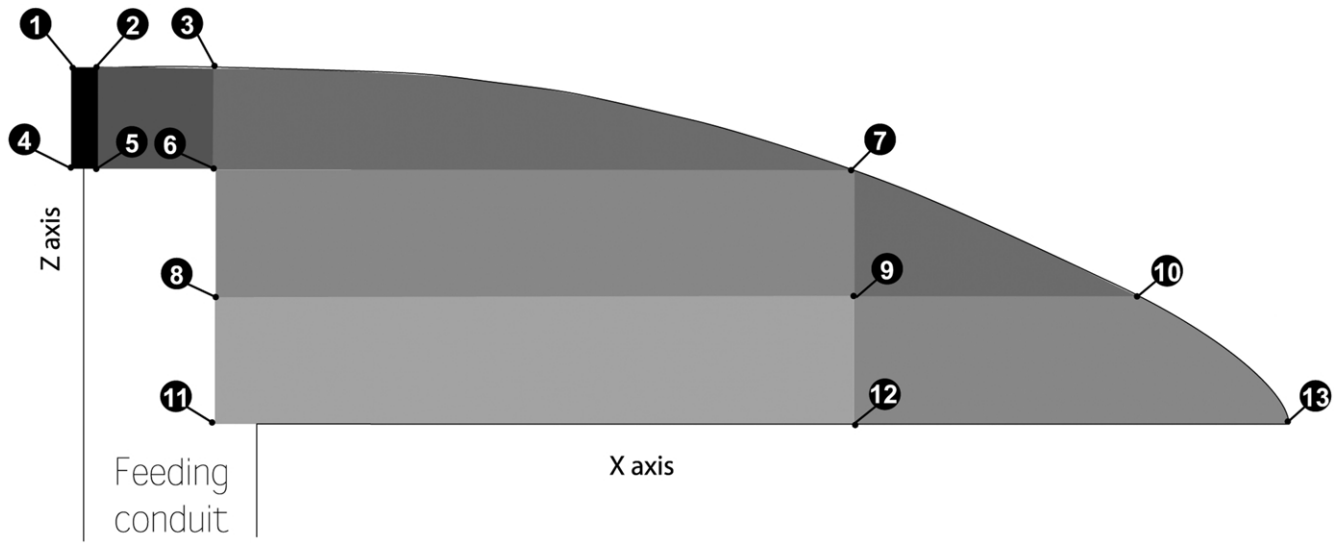

	1	2	3	4	5	6	7	8	9	10	11	12	13
k_X	3	2.3	0.6	7	2	0.30	0.41	0.25	0.83	1.03	0.32	0.9	1.2
k_Y	3	7.5	6	7	7	5.5	3.5	4.5	1.6	1.6	3.5	1.5	1.5
k_Z	0.11	0.058	0.28	0.02	0.07	0.6	0.7	0.9	0.74	0.62	0.9	0.74	0.56
γ_{XZ}	0	0	-2	0	-6	-8	-2	0	5	5	8	13	13
γ_{ZX}	0	0	-0.03	0	-0.06	-0.09	-0.03	-0.095	-0.0125	-0.1125	-0.1	-0.0125	-0.0875

Fig. 2. Specific values of the input parameters used for the numerical simulation at 12 locations on the cross-section (explanation in the text).

the model are everywhere the stretching and shortening axes, respectively. The parameter k_x is a shortening axis in the main part of the model, but becomes a stretching axis when approaching the periphery of the model. Senses of shear are shown in Fig. 1c, as deduced from the deformed squares observed in cross-sections (Buisson and Merle, 2002). It is convenient to divide the cross-section into seven domains. Specific values of strain parameters measured at some locations in the model allow the determination of strain gradients that are used in the numerical simulation (Fig. 2). A full description of the input parameters can be found in Buisson (2001).

Results are shown on a vertical half-section from the feeding conduit in the centre of the dome to the frontal rolling zone (Buisson and Merle, 2002). Deformation being axisymmetrical around the vertical axis passing through the central feeding conduit, any vertical half-section is considered to reveal the same strain pattern, provided that the flow occurs on a horizontal planar base.

3.1. Attitude of flattening planes

The flattening plane is normal to the short axis of the strain ellipsoid and contains the two other strain axes. Results of computations show that the long axis (λ_1) of the strain ellipsoid across the model is either parallel or perpendicular to the vertical section. The attitude of the flattening plane in a vertical section can be reconstructed by plotting either the long (λ_1) or the intermediate (λ_2) axes of the strain ellipsoid across the model.

The orientation of the flattening plane shown in Fig. 3 exhibits a concentric pattern around the feeding conduit, as already observed in experiments (Buisson and Merle, 2002). In a way remarkably similar to experiments, the triple junction between flattening plane trajectories defines a small isotropic triangular area in vertical sections.

3.2. Orientation of stretching axis

The flow direction is parallel to each vertical cross-section. It is vertical above the feeding conduit and then it changes to become sub-horizontal next to the feeding stem. The orientation of the three principal axes of the strain ellipsoid is shown in Fig. 4. Two different domains can be defined. The lower part of the section reveals a stretch axis parallel to the vertical cross-section, which is parallel to the flow direction on a plan view. It dips towards the feeding conduit and becomes more and more flat with time as strain increases. In contrast, the stretch axis is perpendicular to the vertical cross-section in the upper part of the model, which is perpendicular to the flow direction on a plan view. The limit between the two zones is a sloping line that starts from the basal plane next to the feeding conduit and merges upward to the front of the model. In three dimensions, this makes it possible to infer a concentric stretching in the upper part of the flow and a radial stretching in the lower part of the flow.

The distribution of the stretching within the flow is due to the relative magnitude of the three strain components, which are simultaneously combined in the numerical simulation. As already shown for radial flow (Merle, 1998), the 3D coaxial component (k) generates a concentric stretching perpendicular to the flow direction, whereas the two simple shear components (γ_{xz} and γ_{zx}) generate a radial stretching parallel to the flow. Local proportions of k and γ components therefore control whether stretching is concentric or radial. The significant increase of the γ_{xz} component near the base of the model explains the parallelism between stretching and displacement in the lower part of the flow. Similar results in radial flow have been reported both from experiments (Merle, 1998) and natural lava domes (Castro et al., 2002).

3.3. Shape of strain ellipsoid

Computations of the Flinn parameter reveal that K is much smaller than one throughout most of the model indicating flattening type ellipsoids (Fig. 5). However, K values are close to one when approaching the upper free surface of the model, which defines a thin outer zone of plane strain.

The most spectacular result of this simulation is a zone of constriction-type ellipsoids ($K > 1$) located around the isotropic area defined in section by the triple junction of the flattening planes (Fig. 5). K values as high as 63 can be observed in this zone where there is no planar fabric. This indicates that the isotropic area in vertical section is not a zone of low strain. It is best described as a constriction zone, a kind

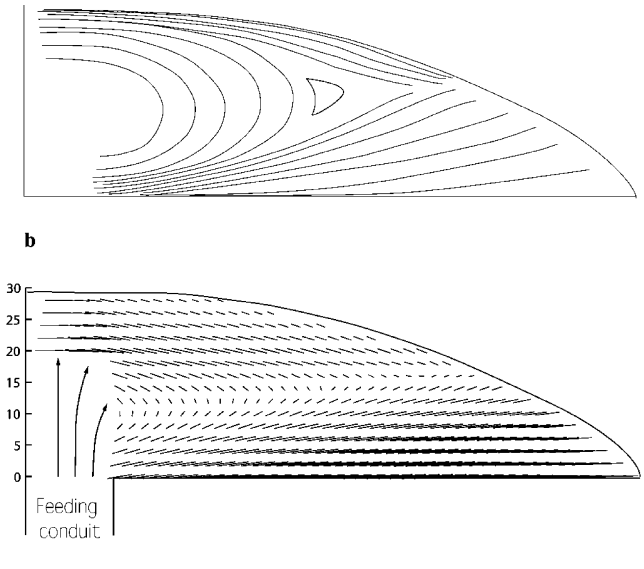

Fig. 3. (a) Orientation of the flattening planes in vertical section. (b) Simplified flattening plane trajectories as deduced from the simulation. Note the triple junction of the trajectories that defines an isotropic area in the strain field (shaded area).

of horizontal tube with stretching parallel to it and oriented perpendicular to the vertical section (i.e. concentric).

4. Limitations of the model

As explained in Buisson and Merle (2002), 2D experiments have been conducted with an isothermal Newtonian fluid, which cannot be considered as a perfect analogue of the magma behaviour in natural domes. These experiments, however, were the first attempt ever done to investigate the internal strain in vertical cross-section of a lava dome. Starting from first principles, it has been shown that scale modelling using a Newtonian fluid is likely to give a basic estimate of the evolving internal strain within a dome, which would be refined when more appropriate experimental procedures are implemented. As the numerical simulation was made from strain gradients observed in the experiments, the same limitation should be expressed regarding the results. The 3D strain pattern calculated in

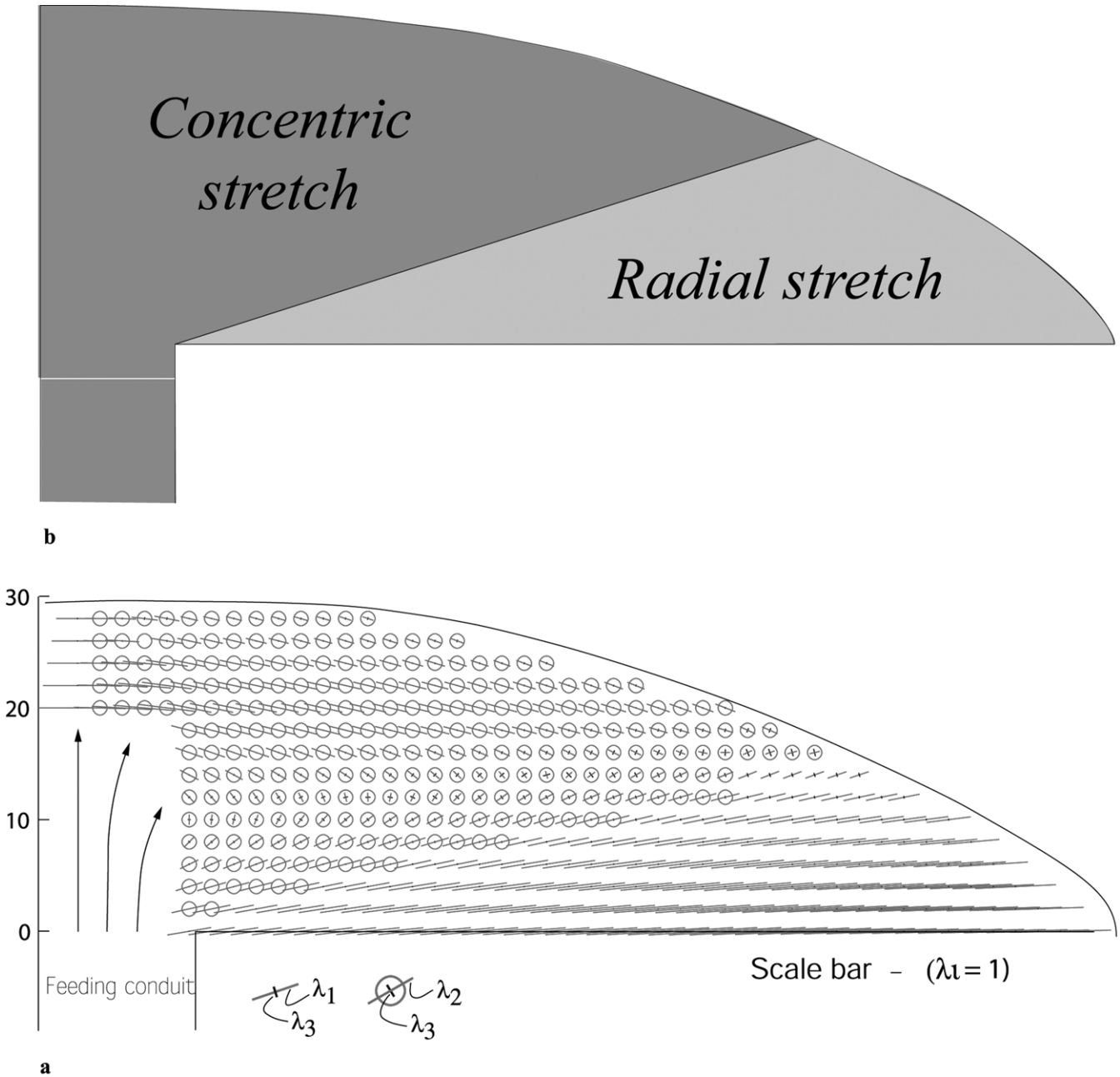

Fig. 4. (a) Orientations and magnitudes of the three main axes of the strain ellipsoid. Circles mean that the stretching axis (λ_1) is perpendicular to the section and that the magnitudes of the least (λ_3) and intermediate (λ_2) strain axes are shown together. When the stretching is parallel to the section, the intermediate axis (λ_2) is normal to the section and its magnitude is not shown. (b) Spatial distribution of radial and concentric stretching fields within a (half) vertical section of a lava dome.

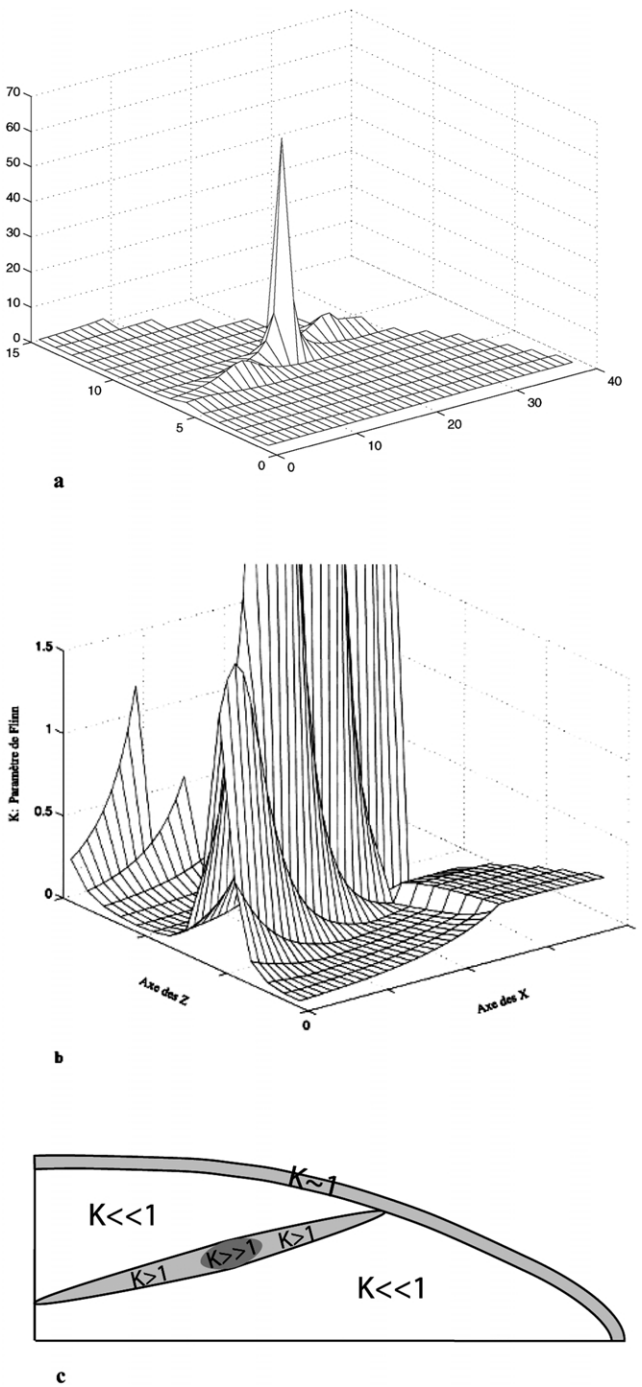

Fig. 5. (a) Spatial distribution of the Flinn parameter (K) in the model. (b) Enlarged view of the diagram showing that the Flinn parameter (K) is close to one when approaching the upper free surface. (c) Cross-section showing the distribution of the Flinn parameter expected in the lava dome.

this paper is the one that could have been observed in experiments if 3D measurements had been possible.

5. Concluding remarks

The study of strain in lava domes provides the opportunity to test a new numerical method to compute the strain pattern in geological structures. This method presented in detail in a companion paper (Provost et al., 2004) allows the calculation of any simultaneous combination of simple shear and pure shear components. It is especially useful when the simultaneous deformation is not expressed by an upper triangular matrix, a condition that has to be fulfilled for previous proposed solutions (Tikoff and Fossen, 1993).

The numerical simulation of strain in lava domes gives further information on the kinematics of dome emplacement, not available from the 2D experiments (Buisson and Merle, 2002). Whereas the flattening plane trajectories are remarkably similar to those obtained from analogue modelling, this study shows that the stretching is concentric in the upper part of the dome, which is perpendicular to the radial direction of flow. The strain is of flattening type ($K < 1$) throughout most of the dome, except in a small triangular zone where it is of constriction type ($K > 1$).

Acknowledgements

We would like to thank Hemin Koyi and Jean de Bremond d'Ars for their helpful reviews of the manuscript.

References

Brun, J.P., 1977. Cumulative strain and boundary effects in the gravity flow of a viscous slab. Tectonophysics 41, T7–T14.

Brun, J.P., Burg, J.P., 1982. Combined thrusting and wrenching in the Ibero–Armorican arc: a corner effect during continental collision. Earth and Planetary Science Letters 61, 319–332.

Buisson, C., 2001. Cinématique et déformation dans les dômes de lave: modélisation analogique et numérique. Ph.D. thesis, University of Clermont-Ferrand.

Buisson, C., Merle, O., 2002. Experiments on internal strain in lava dome cross-sections. Bulletin of Volcanology 64, 363–371.

Castro, J., Manga, M., Cashman, K., 2002. Dynamics of obsidian flows inferred from microstructures: insights from microlite preferred orientations. Earth and Planetary Sciences Letters 199, 211–226.

Coward, M.P., 1976. Strain within ductile shear zones. Tectonophysics 34, 181–197.

Coward, M.P., Kim, J.H., 1981. Strain within thrust sheets. In: Thrust and Nappe Tectonics. Geological Society Special Publication 9, pp. 275–292.

Ellis, M., Watkinson, J., 1987. Orogen-parallel extension and oblique tectonics: the relation between stretching lineations and relative plate motions. Geology 15, 1022–1026.

Jones, R.R., Tanner, P.W., 1995. Strain partitioning in transpression zones. Journal of Structural Geology 17, 793–802.

Malvern, L.E., 1969. Introduction to the Mechanics of a Continuous Medium. Prenctice-Hall, Englewood Cliffs, NJ, 713pp.

Merle, O., 1986. Pattern of stretch trajectories and strain rate within spreading–gliding nappes. Tectonophysics 124, 211–222.

Merle, O., 1998. Internal strain within lava flows from analogue modelling. Journal of Volcanological and Geothermal Research 81, 189–206.

Merle, O., 2000. Numerical modelling of strain in lava tubes. Bulletin of Volcanology 62, 53–58.

Merle, O., Gapais, D., 1997. Strains within thrust–wrench zones. Journal of Structural Geology 19, 1011–1014.

Provost, A., Buisson, C., Merle, O., 2004. From progressive to finite deformation, and back. Journal of Geophysical Research, in press.

Ramberg, H., 1975. Particle paths, displacement and progressive strain applicable to rocks. Tectonophysics 28, 137.

Sanderson, D.J., 1982. Models of strain variation in nappes and thrust sheets: a review. Tectonophysics 88, 201–233.

Sanderson, D.J., Marchini, W.R.D., 1984. Transpression. Journal of Structural Geology 6, 449–458.

Soto, J.I., 1997. A general deformation matrix for three dimensions. Mathematical Geology 29, 93–130.

Tikoff, B., Fossen, H., 1993. Simultaneous pure and simple shear: the unifying deformation matrix. Tectonophysics 217, 267–283.

Tikoff, B., Teyssier, C., 1994. Strain modelling of displacement–field partitioning in transpressional orogens. Journal of Structural Geology 16, 1575–1588.